Geophysical Research Letters

RESEARCH LETTER
10.1029/2019GL084889

The Minimum Scale of Grooving on a Recently Ruptured Limestone Fault

K. K. Okamoto[1], E. E. Brodsky[1], C. A. Thom[2], L. Smeraglia[3], and A. Billi[4]

[1]Department of Earth and Planetary Sciences, University of California, Santa Cruz, CA, [2]Department of Earth Sciences, Oxford University, Oxford, England, [3]Dipartimento di Scienze della Terra, Sapienza University of Rome, Rome, Italy, [4]Consiglio Nazionale delle Ricerche, IGAG, Rome, Italy

Key Points:
- Lithological differences between faults explain the varying values of the minimum scale of grooving
- The small-scale fault roughness of a seismogenic fault shows evidence of plastic deformation
- We develop micrometer scale structure from motion combined with Monte Carlo RMS analysis as a high-resolution method to study roughness

Supporting Information:
- Supporting Information S1

Correspondence to:
K. K. Okamoto,
kkokamot@ucsc.edu

Citation:
Okamoto, K. K., Brodsky, E. E., Thom, C. A., Smeraglia, L., & Billi, A. (2019). The minimum scale of grooving on a recently ruptured limestone fault. *Geophysical Research Letters*, *46*. https://doi.org/10.1029/2019GL084889

Received 12 AUG 2019
Accepted 9 OCT 2019
Accepted article online 9 NOV 2019

Abstract Faults have grooves that are formed by abrasion and wear during slip. Recent observations indicate that this grooving is only a large-scale feature, indicating brittle behavior has a length scale limit. The connection between this scale and earthquake behavior remains limited because no examples exist from a proven seismogenic fault. Here, we address this problem and analyze differences in this scale between lithologies to further our understanding of the underlying mechanics. This study uses samples from the Mt. Vettoretto fault collected after the Norcia earthquake of 2016. We imaged fault topography with a white light interferometer and 10 μm resolution structure from motion and then calculated a Monte Carlo version of root mean square roughness. We found a minimum scale of grooving of ~100 μm. In comparing this fault to the Corona Heights fault, we find that this minimum grooving scale is consistent with predictions based on material properties.

Plain Language Summary As two surfaces slide past each other, harder material can cause grooves or scratches to form in the direction of slip. Recent work showed that on a fault, there exists a change in geometry, or roughness, within these grooves that is evidence of a change in how frictional contacts are deformed. At the micrometer scale, these contacts are deforming without breaking. To link this process to earthquakes, we aim to measure this scale on a fault that hosts known earthquakes. Here, we measure roughness on a fault slipped during the 2016 Norcia earthquake using interferometry and photography. We find this scale and show that it is predictable by measuring properties of the fault. This gives a link between laboratory and natural earthquakes by measuring a length scale and a deformation process that is common to both.

1. Introduction

Faults have grooves at the large scale, but it was recently discovered that these key features are missing below the micrometer scale (Candela et al., 2012; Candela & Brodsky, 2016). Since grooves are commonly used as both kinematic indicators (Twiss & Moores, 1992) and forensic clues on rupture processes (Engelder, 1974), determining the scale at which they disappear, that is, the minimum scale of grooving, is an important problem. Specifically, grooving at near-surface conditions is a brittle process (Beste et al., 2004; Engelder & Scholz, 1976; Toy et al., 2017), and its absence suggests a change from brittle failure to another rheological regime to accommodate the large deformations required as asperities of similar size encounter each other under shear. At small scales, Candela and Brodsky (2016) suggested that plastic failure was the preferred deformation mechanism due to the large stress concentrations on small asperities.

In this previous work, measurements were collected from faults with complex exposure histories or laboratory experiments. In other words, none of the faults had known earthquakes, making the connection between a minimum scale of grooving and earthquake rupture limited. This study aims to measure the minimum scale for a recently ruptured fault and additionally uses a contrast in lithology to elucidate the quantitative link between material properties and minimum grooving scale.

In 2016, two large earthquakes, the M_w 6.0 Amatrice event and the M_w 6.5 Norcia event, occurred on 24 August 2016 and 30 October 2016, respectively. Fault samples from the Mt. Vettoretto were collected on 28 November 2016 (42.800728°N, 13.265781°E, Elevation: 1,625 m above sea level; Figure 1a). The Mt. Vettoretto fault is a segment along the Mt. Vettore-Mt. Gorzano normal fault system that generated the 2016–2017 seismic sequence of central Apennines in Italy (Chiaraluce et al., 2017; Liu et al., 2017; Tinti et al., 2016; Wilkinson et al., 2017). At the Earth's surface, the Mt. Vettoretto fault abruptly slipped by about 5 cm during the

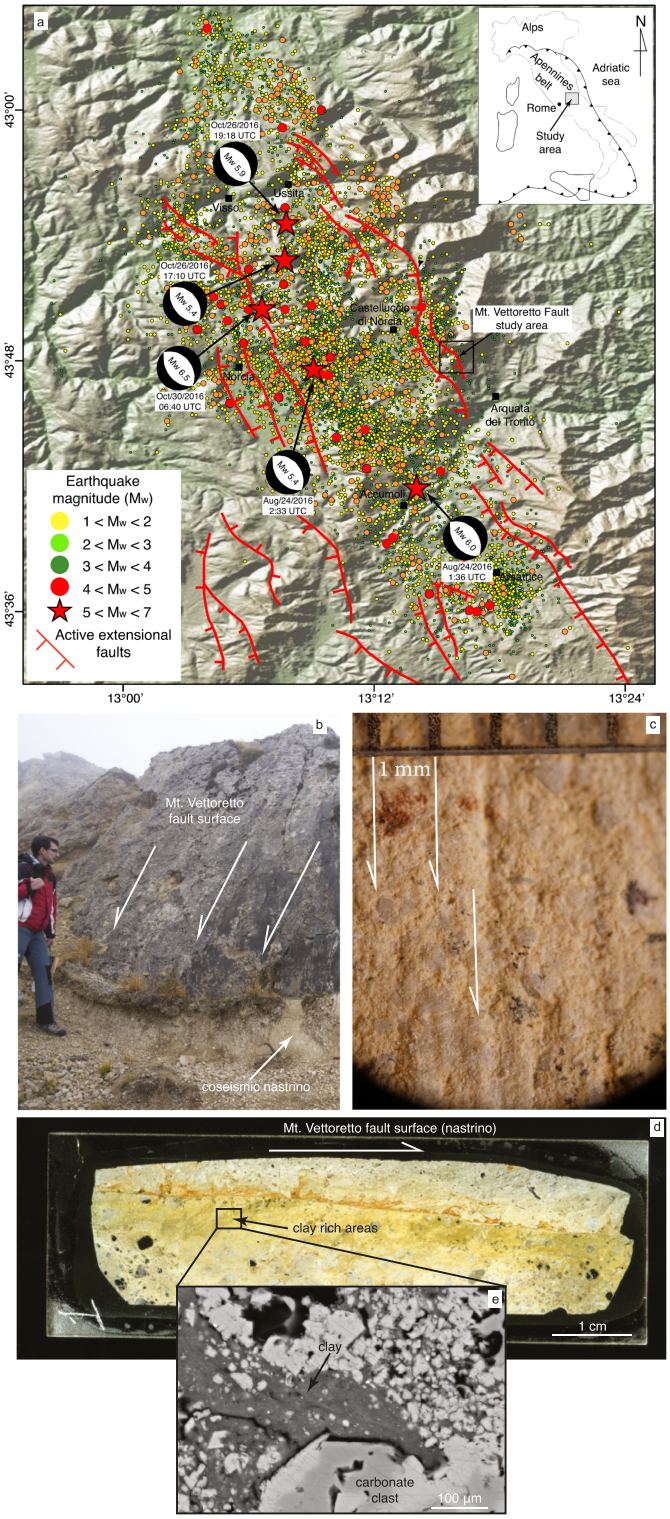

Figure 1. (a) A simplified structural and seismic map of the 2016–2017 central Italian earthquake sequence. The Mt. Vettoretto fault study area where the samples were collected. (b) Coseismic nastrino over the Mt. Vettoretto fault surface mostly generated during the 30 October 2016 M_w 6.5 Norcia earthquake. (c) Microscope photo of a fault sample from the nastrino generated during the 30 October 2016 M_w 6.5 Norcia earthquake. (d) Thin section of a slab across the Mt. Vettoretto fault. (e) Scanning Electron Microscopy image from the previous slab showing a cataclastic mixture of carbonate clasts (white and light grey) and clay (dark grey) along the Mt. Vettoretto fault surface. (Figures 1a, 1d, and 1e are adapted from Smeraglia et al., 2017).

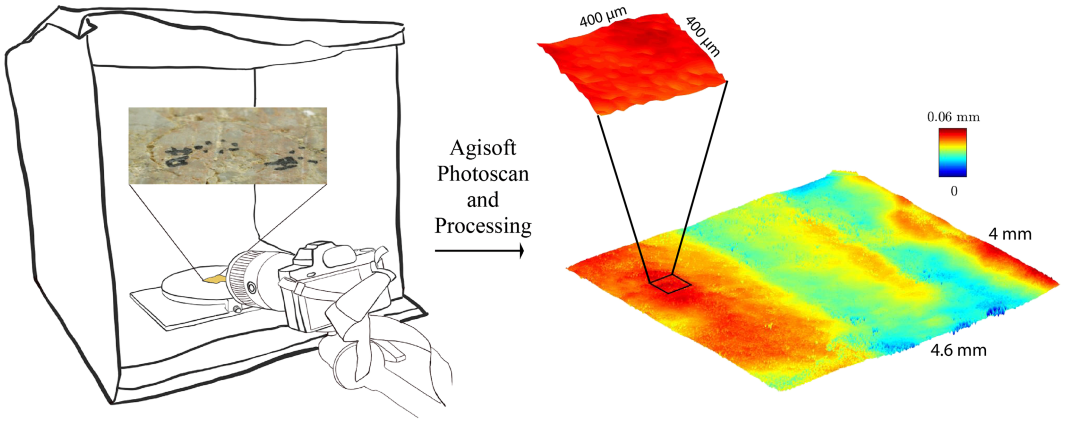

Figure 2. Structure from motion setup for measuring small-scale topography. Lightbox, turntable, and camera depicted. A low angle portion of a photo of the Mt. Vettoretto fault surface, which was used to construct the final topographic map, is shown above sample. The topographic map of structure from motion data shown on the right, this represents one scan of the fault surface. Magnification shows isotropy below the minimum scale of grooving (720 μm for this sample).

Amatrice earthquake and by about 50 cm during the Norcia earthquake. Coseismic surface faulting was demonstrated by displacement of grass and asphalted roads located across the fault. Coseismic displacement was also recorded by near-field Global Navigation Satellite System receivers located in the footwall and hanging wall of the Mt. Vettoretto fault (Wilkinson et al., 2017) and by a clear fresh fault scarp, hereafter referred to as a "nastrino," exhumed along carbonate fault surface (Figure 1b; Smeraglia et al., 2017).

For the roughness measurements, we sampled the striated nastrino freshly exhumed along the fault footwall during the 2016 Amatrice and Norcia earthquakes (Figure 1c). Although there is no direct constraint on the age the striations, roughness is a fragile feature that is commonly destroyed and recreated at each event (Sagy & Brodsky, 2009). It is therefore reasonable to infer that they were formed during the 2016 earthquakes. As previously described by Smeraglia et al. (2017), the footwall of the Mt. Vettoretto fault consists of Jurassic limestone pertaining to the Corniola Formation; however, along the carbonate fault surface, very thin layers of phyllosilicates occur in some areas (Figures 1d and 1e; Smeraglia et al., 2017).

The strategy of this paper is to measure the roughness of striations on fresh fault samples from the Mt. Vettoretto fault and use them to determine the minimum scale of grooving. To achieve the requisite precision over a wide range of scale, we develop a high-resolution measurement procedure for fault roughness based on reconstructing topography from photography and reintroduce scale-dependent root mean square (RMS) roughness measured directly from surfaces as a more appropriate metric for the problem at hand. We then compare the inferred minimum scale of grooving to previous measurements and interpret the results considering lithological and accompanying material property distinctions. Finally, we explore implications for the nucleation of earthquakes on limestone faults.

2. Methods

Hand samples from the Mt. Vettoretto fault were collected following the 30 October M_w 6.5 Norcia earthquake. Cataclasite samples were scanned at UC Santa Cruz using a Zygo NewView 7200 white light interferometer (WLI) with 100X, 50X, and 5X lenses. This produced millimeter-sized topographic maps. To scan centimeter scale patches, we used structure from motion photogrammetry (SFM). We analyzed these topographic maps in the perpendicular and parallel directions with a Monte Carlo version of RMS and then determined the minimum scale of grooving.

For SFM, we used a turntable and macro photographic techniques to capture photos of our hand samples (Figure 2). This is a method for a scale of topography that has previously been difficult to access, and therefore we document it in some detail here. Roughness using structure from motion has previously been analyzed at the millimeter and larger scale (Corradetti et al., 2017; Wilkinson et al., 2016) as well as through focus stacking for submillimeter scales (Olkowicz et al., 2019). Here, we do not use focus stacking but are still

able to achieve submillimeter results. The camera's sensor has an area of 864 mm^2 and 42.4 megapixels, and the photos were taken with a 1:1 macro lens. This allows for a maximum resolution of 4 μm. To capture this resolution, we used the smallest ISO to limit noise, an aperture close to f16, and the longest possible shutter speed without overexposure. Too small of an aperture may contribute to increased noise due to diffraction (Harnischmacher, 2016). We loaded the photos into Agisoft Photoscan Professional to construct dense point clouds. SlugView, a program for viewing and editing point clouds (https://websites.pmc.ucsc.edu/~seisweb/SlugView/Slugview.html), was used to crop the point clouds to only include the most well-resolved area (see supporting information). The resulting point clouds have an approximate resolution of 10 μm.

For both structure from motion and white light interferometer data, we calculated the average RMS of 1-D profiles to characterize roughness. RMS analysis uses a moving window ranging in size from the resolution of the data set to the length of a profile in the data set. A major weakness of RMS roughness in the past is that it is computationally intensive. Here, we developed a Monte Carlo approach that is tractable on current widely available computers (see supporting information Figure S3).

We used the Monte Carlo method to randomly sample each row in both the perpendicular and parallel directions. For each window size, we sampled 20 out of all possible windows for each row and calculated their RMS height. This creates roughness profiles with substantially less noise than traditional power spectra, thus allowing for a clearer view of the isotropic-anisotropic transition. In addition, it avoids the assumptions inherent in both Fourier analysis and Parseval's theorem to transform between power spectral density and RMS height (Brodsky et al., 2011). The Monte Carlo approach also uses the same number of windows for each scale, which avoids the change in uncertainty as a function of scale that would arise if the maximum possible number of windows were used at each scale.

Using this Monte Carlo version of RMS, we analyzed the Mt. Vettoretto fault samples. We determined the minimum scale of grooving (L_c) by locating the length scale where there is a 10% difference between the slip perpendicular roughness and slip parallel roughness (Figure 3a). Candela and Brodsky (2016) measured Lc at the location where slip parallel roughness was at least 30% of slip perpendicular roughness as measured by power spectral density. The variability of Monte Carlo RMS roughness is lower than that of power spectral density roughness because RMS roughness is related to the integrated power spectral density over a band of frequencies and, so the anisotropic-isotropic transition can be measured closer to convergence. The critical height, H_c, is the RMS roughness at the critical length scale, L_c.

3. Observed Minimum Scale of Grooving

The RMS roughness of the slip parallel and slip perpendicular converge at an average critical length scale, L_c, 190 μm ± 88 μm (one standard deviation) for the Mt. Vettoretto fault samples (Figure 3a). The variability in L_c is similar to those found by Candela and Brodsky (2016) where they measured faults with an order of magnitude difference between the smallest and largest L_c values. Despite this variability in L_c, the data fall on a line of critical aspect ratio (H_c/L_c). This critical aspect ratio spans from 1.7–3.2% over a 95% confidence interval with a mean of 2.5%. This amount of variability in the critical aspect ratio is again consistent with Candela and Brodsky (2016).

The structure from motion L_c values falls on a slightly lower critical aspect ratio trendline than the white light interferometer (Figure 3a). For the white light interferometry, we focused on imaging the grooves along the fault, and therefore, there may have been a sampling bias of the rougher portions of the fault. For structure from motion, the topographic maps were significantly larger enabling the inclusion of areas with smoother roughness than what was focused on using the WLI. This inherent sampling bias could have contributed to a higher critical aspect ratio for the white light data and a lower one for the structure from motion. The focus of this study is the range of L_c and this is the same between the SFM and WLI data sets, so this sampling bias does not affect our overall results.

4. Interpretation of the Minimum Scale of Grooving as a Sign of Plasticity

The Mt. Vettoretto samples stand out as having larger values of L_c than other faults (Figure 3). They also have the largest value of H_c/L_c of 1.7–3.2%. Intriguingly, the two faults with the largest L_c are Mt. Vettoretto fault, analyzed here, and the Bolu fault, are both composed of limestone. They both have L_c on

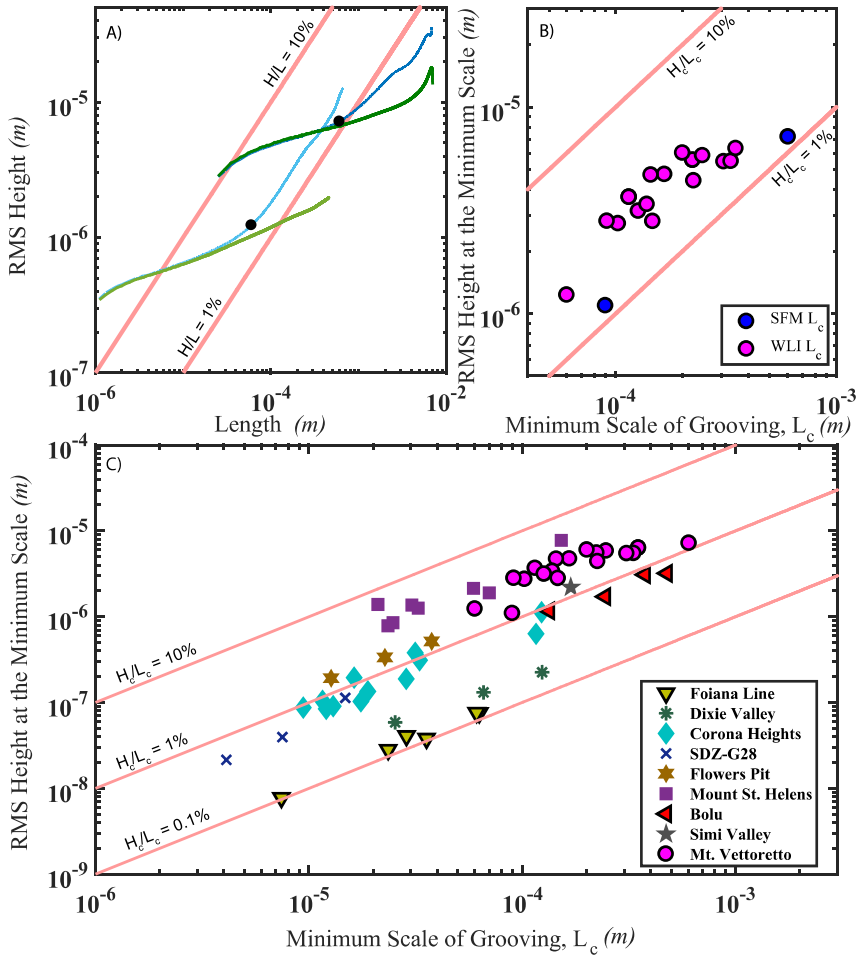

Figure 3. (a) Root mean square height (H) versus wavelength (L) for the Mt. Vettoretto fault. The root mean square height in both perpendicular (blue lines) and parallel (green lines) to slip for chosen scans of the fault. (b) The minimum scale of grooving(L_c) for the Mt. Vettoretto fault measured by white light interferometer (pink) and structure from motion (blue). (c) The minimum scale of grooving for the Mt. Vettoretto fault (pink circles) compared to the faults analyzed by Candela and Brodsky (2016). Carbonate faults are outlined in black. Note that although the Foiana Line fault is a carbonate, it is composed of dolomite. The red lines indicate reference aspect (H_c/L_c) ratios as annotated. (Figure adapted from Candela & Brodsky, 2016 with additional data from this study). RMS = root mean square; SFM = structure from motion photogrammetry; WLI = white light interferometer.

the order of 100 μm, while the L_c of previously analyzed silicate and dolomite faults mostly falls in the tens of micrometers range. Can material properties explain the lithological difference in L_c?

We test whether this observation is consistent with the thinking that brittleness should control the minimum grooving length. For an elasto-plasto-brittle material, brittle fracture occurs when the stress intensity factor describing the elastic stress concentration at the edge of an incipient fracture exceeds a critical value determined by the material. Plastic yielding occurs when the elastic stresses exceed a yield stress, which is also a material property. The brittle-plastic transition defines which failure mechanism is preferred when an initially elastic loading results in failure. Lawn and Marshall (1979) showed that during an indentation test, which is analogous to an asperity collision, the scale of the minimum length crack that experiences brittle rather than plastic failure is c_m and it depends on material properties according to

$$c_m = \alpha K_c / {\sigma_c}^2 \tag{1}$$

where α is a geometrical constant, K_c is the critical stress intensity factor (toughness), and σ_y is the plastic yield stress of the material at the length scale of the minimum scale of grooving. This scale, c_m, is also

related to the definition of a fracture process zone and is a general feature of elasto-plasto-brittle material (Barenblatt, 1962; Kendall, 1978; Lawn, 1993; Mouginot, 1988; Puttick, 1980). Does this relationship also explain the minimum scale of grooving, that is, is L_c equal to c_m?

The constant of proportionality, α, in equation ((1)) depends on the details of the stressor geometry, which makes it difficult to test the predicted value for a single fault. Instead, we take the strategy of comparing two faults with different material properties and test whether the ratio of minimum grooving scales corresponds to the predictions of equation ((1)). Qualitatively, equation (1) predicts that more brittle rocks should have a smaller minimum scale of grooving than less brittle ones, like calcite. The comparison between the calcite-hosted Mt. Vettoretto fault studied here and the chert-hosted Corona Heights fault previously studied provides an opportunity to test the prediction both qualitatively and quantitatively.

We calculate $(K_c/\sigma_y)^2$ for the fault rocks of both Mt. Vettoretto and Corona Heights and then determine how the ratio of the two compares to the ratio of the minimum scale of grooving. We used values of yield strength from indent tests extrapolated to the critical length scale. Measurements of Mt. Vetteorretto were done for this study (see supporting information), and values for Corona Heights were available from a previous study (Thom et al., 2017). The resulting yield stress is 0.3 and 4.6 GPa, respectively, for Mt. Vettoretto and Corona Heights. We used measurements of Mode I fracture toughness from the literature assuming Mt. Vettoretto is mostly calcite (Smeraglia et al., 2017), while Corona Heights is mostly quartz (Kirkpatrick et al., 2013). The critical stress intensity factor for Mode I failure, K_{Ic}, is equal to 0.39 MPa·m$^{1/2}$ for dry calcite and 1.6 MPa·m$^{1/2}$ for dry quartz (Broz et al., 2006). Mode II fracture toughness would be a better metric for the type of failure on the fault, but few values are available and we look forward to greater characterization in the future of this important parameter. We use these values and equation ((1)) to predict the ratio of L_c between the two faults should equal 12. The actual mean ratio of L_c between Mt. Vettoretto and Corona Heights, as measured from topographic data, is 8.9 and 90% of the ratios are between 2.4 and 25. The agreement between the two values is further evident that the minimum scale of grooving is a proxy for the brittle-plastic transition.

Toy et al. (2017) recently proposed pressure solution as an alternative explanation to plastic deformation for a mechanism for slickenline development at high temperatures and suggested that the brittle-plastic transition discussed here was inapplicable at those conditions because plastic yield was not reached for the stresses studied. Although pressure solution may indeed be an important process, the calculations presented in Toy et al. (2017) only considered the squeeze of asperities under an average normal stress equal to the load divided by the apparent area of contact. Those calculations are inappropriate for the brittle-plastic transition as discussed here as the deformation is due to asperity collision under shear with stress concentrated on the real area of contact.

5. Implications of the Minimum Scale of Grooving for Limestone Faults

The minimum scale of grooving appears to mark the brittle-plastic transition, and this observation may have an implication for friction. Dieterich and Kilgore (1994) found that the mean size of individual viscoplastic, creeping contacts is approximately equal to the critical slip distance, D_c. They imposed the asperity scale through polishing with a specific size grit, which left open the question of which asperity size controls friction for a multiscale surface like a natural fault. If there is a maximum scale of plastic deformation possible under shear, then this scale could also be the relevant control on D_c. In other words, both D_c and L_c may be controlled by the same process.

As a first check on this hypothesis, we can compare values of D_c for limestone and silicates as measured in the laboratory. The critical slip distance is typically measured experimentally through velocity-stepping experiments. Carpenter et al. (2014) measured *Dc* on limestone from the Monte Maggio fault with a normal stress of 10 MPa. For experiments sliding between two solid surfaces, between gouge and solid surface, and in gouge, they found *Dc* ranging from 5–125 μm, 60–220 μm, and 65–160 μm, respectively. We can compare these results to granite experiments using the same apparatus with normal stresses of 5 and 10 MPa. For these, D_c ranged from 0.1–7.5 μm and 8–16 μm for sliding between two solid surfaces and within gouge, respectively (Savage & Marone, 2008). Monte Maggio's critical slip distance is greater than that of the granite for both surfaces and gouge, suggesting that D_c is greater for faults composed of limestone than for those composed of silicates. The laboratory dependencies on lithology are consistent with the minimum grooving scale.

The connection between the minimum scale of grooving and the slip weakening scale, D_c, is significant because of the role that slip weakening plays in controlling earthquake nucleation (Scholz, 1998; Rubin & Ampuero, 2005). Note that this microscopic slip weakening distance utilized in classical nucleation models is distinct from any further dynamic weakening that occur at seismic slip rates (Di Toro et al., 2011). As such, it should not be confused with seismic measurements of high-speed weakening (Tinti et al., 2005). Despite the importance of D_c, constraints on its value and even existence in nature are limited. Our results indicate that the minimum scale of grooving may be the first geological tool available to determine D_c from natural faults and highlights the relevance of laboratory friction in understanding real faults. The tool can be used wherever there is a well-defined slip surface in either the intact rock or embedded in gouge. Future samples from depths of nucleation can now use this method to constrain D_c and compare it to theory.

The high minimum scale of grooving observed for limestone faults suggests a particular role for lithology in determining nucleation. Even though the nucleation zone is not directly sampled here, the potential connection between bulk material properties and frictional behavior predicts a difference in nucleation between limestone and silicate rocks. A larger D_c favors stable sliding by reducing the critical stiffness that needs to be exceeded to eliminate stick slip when $(a–b) < 0$, the condition for unstable nucleation where a and b are the parameters governing rate and state dependence of friction, respectively (Rabinowicz, 1958; Scholz, 1998). In addition, for a larger D_c, the stability transition will occur at a larger nucleation length (Scholz, 1998). All else being equal, the lithological dependence of the brittle-plastic transition suggests that critical nucleation lengths for limestone faults may be larger than for faults composed of silicate and dolostone. Additional factors such as gouge thickness, fluid content, mesoscale structures, pressure, and temperature may complicate the situation in real faults where all else is seldom equal (Colletini et al., 2011; Marone & Kilgore, 1993; Scholz, 2002).

6. Conclusion

The minimum scale of grooving is identified for a recently ruptured fault further supporting that it is the geological imprint of the cross-over from plastic to brittle behavior. To make these measurements, we developed an approach for high-resolution roughness analysis: small-scale structure from motion combined with Monte Carlo RMS, allowing for analysis of small-scale roughness to be more affordable and less computationally intensive. In addition to our finding on the observability of the minimum scale, these measurements are the largest yet observed. Comparing the yield strength and fracture toughness of the Mt. Vettoretto fault to the Corona Heights fault explains this large minimum scale. This suggests that limestone faults, like the Mt. Vettoretto fault, have a larger critical slip distance than silicate faults under similar conditions.

Acknowledgments
We thank L. Malatesta and S. Dalbesio for photographic equipment and assistance. This work was funded by the Hierarchical Systems Foundation, the Smith Renaissance Society, and NSF award EAR-1624657. Further information on methods for indentation testing, Monte Carlo RMS, and structure from motion is available in the supplements. The function for running a Monte Carlo version of RMS is on github.com/kkokamot/MinScale. The data and results of our analysis are available at https://doi.org/10.5281/zenodo.3364708

References

Barenblatt, G. I. (1962). The mathematical theory of equilibrium cracks in brittle fracture. *Advances in Applied Mechanics*, *7*, 55–129. https://doi.org/10.1016/S0065-2156(08)70121-2

Beste, U., Lundvall, A., & Jacobson, S. (2004). Micro-scratch evaluation of rock types—A means to comprehend rock drill wear. *Tribology International*, *37*(2), 203–210. https://doi.org/10.1016/S0301-679X(03)00038-0

Brodsky, E. E., Gilchrist, J., Sagy, A., & Colletini, C. (2011). Faults smooth gradually as a function of slip. *Earth and Planetary Science Letters*, *302*(1-2), 185–193. https://doi.org/10.1016/j.epsl.2010.12.010

Broz, M. E., Cook, R. F., & Whitney, D. F. (2006). Microhardness, toughness, and modulus of Mohs scale minerals. *American Mineralogist*, *91*(1), 135–142. https://doi.org/10.2138/am.2006.1844

Candela, T., & Brodsky, E. E. (2016). The minimum scale of grooving on faults. *Geology*, *44*(8), 603–606. https://doi.org/10.1130/G37934.1

Candela, T., Renard, F., Klinger, Y., Mair, K., Schmittbuhl, J., & Brodsky, E. E. (2012). Roughness of fault surfaces over nine decades of length scales. *Journal of Geophysical Research*, *117*, B08409. https://doi.org/10.1029/2011JB009041

Carpenter, B. M., Scuderi, M. M., Colletini, C., & Marone, C. (2014). Frictional heterogeneities on carbonate-bearing normal faults: Insights from the Monte Maggio Fault, Italy. *Journal of Geophysical Research: Solid Earth*, *119*, 9062–9076. https://doi.org/10.1002/2014JB011337

Chiaraluce, L., Di Stefano, R., Tinti, E., Scognamiglio, L., Michele, M., Casarotti, E., et al. (2017). The 2016 Central Italy seismic sequence: A first look at the mainshocks, aftershocks, and source models. *Seismological Research Letters*, *88*(3), 757–771. https://doi.org/10.1785/0220160221

Colletini, C., Niemeijer, A., Viti, C., Smith, S. A. F., & Marone, C. (2011). Fault structure, frictional properties and mixed-mode faulting. *Earth and Planetary Science Letters*, *311*(3-4), 316–327. https://doi.org/10.1016/j.epsl.2011.09.020

Corradetti, A., McCaffrey, K., De Paola, N., & Tavani, S. (2017). Evaluating roughness scaling properties of natural active faul surfaces by means of multi-view photogrammetry. *Tectonophysics*, *717*, 599–606. https://doi.org/10.1016/j.tecto.2017.08.023

Di Toro, G., Han, R., Hirose, T., De Paola, N., Nielsen, S., Mizoguchi, K., et al. (2011). Fault lubrication during earthquakes. *Nature*, *471*(7339), 494–498. https://doi.org/10.1038/nature09838

Dieterich, J. H., & Kilgore, B. D. (1994). Direct observation of frictional contacts: New insights for state-dependent properties. *Pure and Applied Geophysics*, *143*(1-3), 283–302. https://doi.org/10.1007/BF00874332

Engelder, J. T. (1974). Microscopic wear grooves on slickensides: Indicators of paleoseismicity. *Journal of Geophysical Research*, *79*(29), 4387–4392. https://doi.org/10.1029/JB079i029p04387

Engelder, J. T., & Scholz, C. H. (1976). The role of asperity indentation and ploughing in rock friction—II: Influence of relative hardness and normal load. *International Journal of Rock Mechanics and Mining Science and Geomechanics Abstracts*, *13*(5), 155–163. https://doi.org/10.1016/0148-9062(76)90820-2

Harnischmacher, C. (2016). "The Basics in Theoretical Terms". In *The Complete Guide to Macro and Close-Up Photography* (pp. 7–16). Santa Barbara: Rocky Nook Inc. Print.

Kendall, K. (1978). Complexities of compression failure. *Proceedings of the Royal Society A.*, *361*(1705), 245–263. https://doi.org/10.1098/rspa.1978.0101

Kirkpatrick, J. D., Rowe, C. D., White, J. C., & Brodsky, E. E. (2013). Silica gel formation during fault slip: Evidence form the rock record. *Geology*, *41*(9), 1015–1018. https://doi.org/10.1130/G34483.1

Lawn, B. R. (1993). *Fracture of brittle solids*. Cambridge: Cambridge University Press.

Lawn, B. R., & Marshall, D. B. (1979). Hardness, toughness, and brittleness: An indentation analysis. *Journal of the American Ceramic Society*, *89*(6), 435–350. https://doi.org/10.6028/jres.089.024

Liu, C., Zheng, Y., Xie, Z., & Xiong, X. (2017). Rupture features of the 2016 Mw 6.2 Norcia earthquake and its possible relationship with strong seismic hazards. *Geophysical Research Letters*, *44*, 1320–1328. https://doi.org/10.1002/2016GL071958

Marone, C., & Kilgore, B. (1993). Scaling of the critical slip distance for seismic faulting with shear strain in fault zones. *Nature*, *362*(6421), 618–621. https://doi.org/10.1038/362618a0

Mouginot, R. (1988). Blunt or sharp indenters: A size transition analysis. *Journal of the American Ceramic Society*, *71*(8), 658–661. https://doi.org/10.1111/j.1151-2916.1988.tb06384.x

Olkowicz, M., Dabrowski, M., & Pluymaker, A. (2019). Focus stackingphotogrammetry for micro-scale roughness reconstruction: A methodological study. *The Photogrammetric Record*, *34*(165), 11–35. https://doi.org/10.1111/phor.12270

Puttick, K. E. (1980). The correlation of fracture transitions. *Journal of Physics D: Applied Physics*, *13*(12), 2249–2262. https://doi.org/10.1088/0022-3727/13/12/011

Rabinowicz, E. (1958). The intrinsic variables affecting the stick-slip process. *Proceedings of the Physical Society*, *71*(4), 668–675. https://doi.org/10.1088/0370-1328/71/4/316

Rubin, A. M., & Ampuero, J. P. (2005). Earthquake nucleation on (aging) rate and state faults. *Journal of Geophysical Research*, *110*, B11312. https://doi.org/10.1029/2005JB003686

Sagy, A., & Brodsky, E. E. (2009). Geometric and rheological asperities in an exposed fault zone. *Journal of Geophysical Research*, *114*, B02301. https://doi.org/10.1029/2008JB005701

Savage, H. M., & Marone, C. (2008). Potential for earthquake triggering from transient deformations. *Journal of Geophsyical Research*, *113*, B05302. https://doi.org/10.1029/2007JB005277

Scholz, C. H. (1998). Earthquakes and friction laws. *Nature*, *391*(6662), 37–42. https://doi.org/10.1038/34097

Scholz, C. H. (2002). *The mechanics of earthquakes and faulting*. Cambridge: Cambridge University Press.

Smeraglia, L., Billi, A., Carminati, E., Cavallo, A., & Doglioni, C. (2017). Field- to nano-scale evidence for weakening mechanisms along the fault of the 2016 Amatrice and Norcia Earthquakes, Italy. *Tectonophysics*, *712-713*, 156–169. https://doi.org/10.1016/j.tecto.2017.05.014

Thom, C. A., Brodsky, E. E., Carpick, R. W., Pharr, G. M., Oliver, W. C., & Goldsby, D. L. (2017). Nanoscale roughness of natural fault surfaces controlled by scale-dependent yield strength. *Geophysical Research Letters*, *44*, 9299–9307. https://doi.org/10.1002/2017GL074663

Tinti, E. P., Scognamiglio, L., Michelini, A., & Cocco, M. (2016). Slip heterogeneity and directivity of the ML 6.0, 2016, Amatrice earthquake estimated with rapid finite-fault inversion. *Geophysical Research Letters*, *43*, 10,745–10,752. https://doi.org/10.1002/2016GL071263

Tinti, E. P., Spudich, P., & Cocco, M. (2005). Earthquake fracture energy inferred from kinematic rupture models on extended faults. *Journal of Geophysical Research*, *110*, 303. https://doi.org/10.1029/2005JB003644

Toy, V. G., Niemeijer, A., Renard, F., Morales, L., & Wirth, R. (2017). Striation and slickenline development on quartz fault surfaces at crustal conditions: Origin and effect on friction. *Journal of Geophysical Research: Solid Earth*, *122*, 3497–3512. https://doi.org/10.1002/2016JB013498

Twiss, R. J., & Moores, E. M. (1992). *Structural geology*. San Francisco, CA: Freeman, W. H. & Company.

Wilkinson, M. W., Jones, R. R., Woods, C. E., Gilment, S. R., McCaffrey, K. J. W., Kokkalas, S., & Long, J. J. (2016). A comparison of terrestrial laser scanning and structure-from-motion photogrammetry as methods for digital outcrop acquisition. *Geosphere*, *12*(6), 1865–1880. https://doi.org/10.1130/GES01342.1

Wilkinson, M. W., McCaffrey, K. J. W., Jones, R. R., Roberts, G. P., Holdsworth, R. E., Gregory, L. C., et al. (2017). Near-field fault slip of the 2016 Vettore Mw 6.6 earthquake (Central Italy) measured using low-cost GNSS. *Scientific Reports*, *7*(1), 4612. https://doi.org/10.1038/s41598-017-04917-w